Decadal Terminus Position Changes and Ice Thickness Measurement of Menthosa Glacier in Lahaul Region of North-Western Himalaya

Article *in* Geocarto International · June 2021

DOI: 10.1080/10106049.2021.1939437

CITATIONS
2

READS
287

11 authors, including:

Satya Prakash
Jawaharlal Nehru University
12 PUBLICATIONS **49** CITATIONS
SEE PROFILE

Milap C Sharma
Jawaharlal Nehru University
83 PUBLICATIONS **2,022** CITATIONS
SEE PROFILE

Pritam Chand
Central University of Punjab
30 PUBLICATIONS **497** CITATIONS
SEE PROFILE

Vijendra Kumar Pandey
Kirori Mal College University of Delhi
23 PUBLICATIONS **161** CITATIONS
SEE PROFILE

GEOCARTO INTERNATIONAL
https://doi.org/10.1080/10106049.2021.1939437

Taylor & Francis
Taylor & Francis Group

Decadal terminus position changes and ice thickness measurement of Menthosa Glacier in Lahaul region of North-Western Himalaya

Satya Prakash[a,b], Milap Chand Sharma[a], S. Sreekesh[a], Pritam Chand[c], Vijendra Kumar Pandey[d], Syed Umer Latief[a,e], Sanjay Deswal[f], Ishita Manna[a], Suresh Das[a], Sandip Tanu Mandal[a] and I. M. Bahuguna[g]

[a]Centre for the Study of Regional Development, School of Social Sciences, Jawaharlal Nehru University, New Delhi, India; [b]Department of Geography, Government College Chowari, Chamba, Himachal Pradesh, India; [c]Department of Geography, School of Environment and Earth Sciences, Central University of Punjab, Bathinda, India; [d]Department of Geography, Kirori Mal College, New Delhi, India; [e]P.G. Department of Geography, Amar Singh College Srinagar, Srinagar, India; [f]Department of Geography, Government College Dujana, Jhajjar, Haryana, India; [g]Space Application Centre, Ahmedabad, India

ABSTRACT

Glacier ice-thickness measurement and distribution is one of the essential variables to assess present status of glacier-water equivalent and its volumetric reserve as well as to model the future glacier dynamics under the climate changing scenario. Yet, substantial gaps in ice thickness information exist for the Himalayan glaciers. The present study provides a long-term assessment (1965–2016) of recessional and area change patterns, as well as the detailed field-based (2016–2017) Ground Penetrating Radar(GPR), derived ice-thickness measurement of the Menthosa Glacier, Lahaul Himalaya. Additionally, the study examines whether the modelled ice thickness from remote sensing data is consistent with the field-based GPR measurement and how can it be improved. The extensive field surveys coupled with the multi-temporal high (Corona KH-4A) to medium resolution (Landsat Enhanced Thematic Mapper+ (ETM+)/Operational Land Imager (OLI), Sentinel 2A-Multispectral Instrument (MSI)) remote sensing data and cross-sectional GPR surveyed profile measurements have been used to examine past half a century (1965–2016) glacier fluctuation and the recent ice-thickness estimations, respectively. The results show that the Menthosa Glacier receded by 301.5 ± 19.2 m during the past half a century (1965–2016) with an average annual retreat of 5.9 ± 0.4 m a^{-1}, whereas glacier lost 0.09 km^2 ice in the frontal section. Field measurement over the past one decade (2006–2017) also conforms to a continuous recessional pattern and substantial glacier degeneration particularly the extensive surface lowering and significant appearance of ice-cliffs in the ablation and lateral zones over this period. The GPR measurements (2017) show the

ARTICLE HISTORY
Received 14 August 2020
Accepted 25 May 2021

KEYWORDS
Glacier terminus changes; glacier ice-thickness; Ground Penetrating Radar (GPR); remote sensing; Lahaul Himalaya

CONTACT Satya Prakash satyapthakur@gmail.com

Supplemental data for this article is available online at https://doi.org/10.1080/10106049.2021.1939437.
This article has been republished with minor changes. These changes do not impact the academic content of the article.

minimum glacier ice thickness of 24 meters at 4691 m a.s.l. (in the lower part of ablation area) and maximum glacier ice thickness of 55 meters measured at 4758 m a.s.l. (in the upper left-side tributary part of ablation area). Moreover, the modelled ice thickness derived from remotely sensed data is having Root Mean Square Error (RMSE) between 38 to 72 ± 10 m as compared with GPR measured ice thickness.

1. Introduction

The Himalayan glaciers are the largest storehouse of freshwater resources after the poles (Xu et al. 2009; Immerzeel et al. 2010; Bolch et al. 2012). Therefore, monitoring long-term glacial fluctuations is required in the backdrop of changing climate (Chand et al. 2017; Shekhar et al. 2017), and its widespread effects on downstream population (Maurer et al. 2019; Tawde et al. 2019). The long-term assessments and monitoring of glaciers fluctuations of past and present will provide vital information on future demand for hydro power generation, water supply to agriculture and various ecosystems in glaciated and downstream areas and melting contribution to hydrological process and associated hazards and eventually to regional/global sea-level changes (Latief et al. 2016; Gärtner-Roer et al. 2019; Maurer et al. 2019). Since past five decades, several studies started to estimate the two-dimensional (2D i.e. glacier length or area) glacier changes and reported the continuous recession of glaciers across the Himalayan regions except for few regions in the Karakarom (Bhambri et al. 2011; Bolch et al. 2012; Yao et al. 2012; Qiao and Yi 2017). However, studies suggested that the change in glacier extent provides the rough approximation of response of a glacier to climate change. Hence, the complex relationship between climate and glacier change cannot be merely represented by change in area and length of the glacier (Scherler et al. 2011). Therefore, it is necessary to assess ice thickness of glaciers for measuring water reserves stored in glaciers as well as to comprehend the future glacier behaviour in response to simulated climate change scenarios (Frey et al. 2014). In recent years, remote sensing modelled based methods extensively used to assess ice thickness of glaciers on the global scale (Huss and Farinotti 2012; Farinotti et al. 2019) includes the regional to local-scale assessment across Himalayan–Karakoram region (Frey et al. 2014; Maurer et al. 2019); and especially in the north-western Himalaya (Vincent et al. 2013; Vijay and Braun 2016). However, these modelled based methods are more susceptible to errors compare to in-situ methods majorly due to the use of low resolution dataset (or DEMs), averaging effects (Vijay and Braun 2016), data gaps (Maurer et al. 2019), inaccuracy of used glacier inventories (Nuimura et al. 2015), utilization of glacier specific shape factor value and model parameterization scheme, and post-processing limitations (Kumar et al. 2020). Moreover, there are substantial gaps existed in field-based glacier ice thickness data across the Himalayan region with only few field measured glacier's ice thickness e.g. Chhota Shigri Glacier (Azam et al. 2012), Satopanth Glacier (Mishra et al. 2018), Hamtah and Parang Glacier (Swain et al. 2018) and Patsio Glacier (Singh et al. 2018). Thus, ground-penetrating radar (GPR) based individual glacier ice thickness measurements are required for a better assessment of the glacier's geometry, internal structure, thickness and overall volume and mass. Additionally, in-situ GPR glacier thickness measurements are also notably complement to assess the accuracy and quality of modelled based assessment of glacier's thickness which emerges as an alternative to assess the glacier volume or water storage on local to regional to global scale.

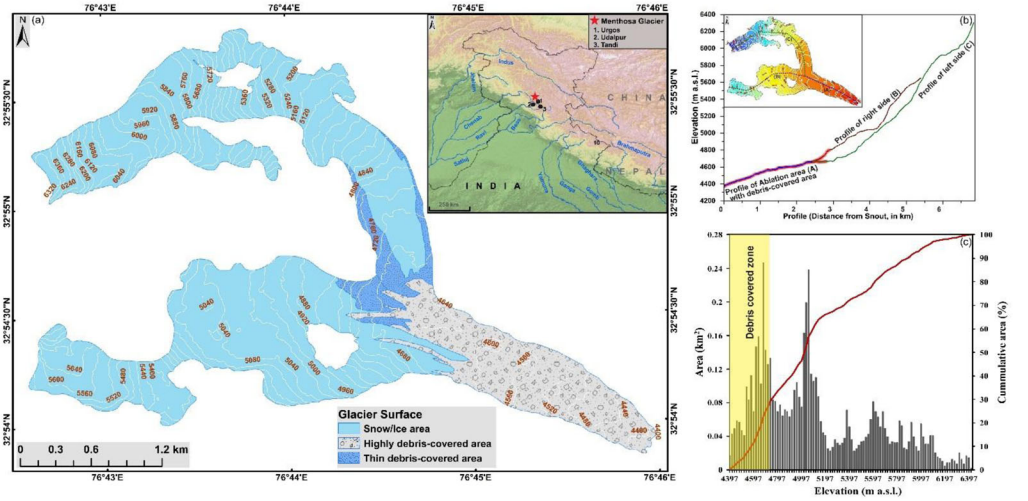

Figure 1. (a) Location of the study area; (b) Elevation profiles of ablation area, right and left side glacier tributaries; (c) Altitudinal characteristics of the Menthosa Glacier.

Field-based study is an essential component of glaciology to cover the complexity of a glacier system and highly desirable and recommended, yet only a few glaciers have been studied using field-based methods in context to glacier terminus change measurements (e.g. Mehta et al. 2011; Chand and Sharma 2015a), mass balance studies (Azam et al. 2012; Pratap et al. 2016) and glacier's ice thickness measurements (Singh et al. 2010; Azam et al. 2012; Singh et al. 2017; Mishra et al. 2018; Singh et al. 2018; Swain et al. 2018) owe to highly inaccessible rugged terrain, logistics and time constraints. Thus, a combination of multi temporal high to medium resolution remote sensing datasets and field-based method, observation and validation is more appropriate to estimate temporal glacier changes, ice thickness and volume of glaciers to understand the overall response of climate change on glacier dynamics. Towards addressing the long-term glacier change and to contribute the field-based ice thickness measurements , the present study aims to examine the long-term (i.e. 1965–2016) changes for the Menthosa Glacier using high-to-medium resolution datasets with supplement of continuous decadal field-based observations (2006 to 2016); to elucidate the possible impacts of climatic factors on glacial changes; and to provide the field-based GPR ice thickness estimates and further to validate the available modelled based ice thickness datasets for this glacier (Farinotti et al. 2019).

2. Study area

The Menthosa Glacier extends between 32°54′1.04″N and 32°55′48.83″N latitudes, 76°42′41.19″E and 76°45′53.93″E longitudes (Figure 1), covering ∼6 km^2 area, having a length of ∼6.7 km (from the left side) dropping down from 6351 m (just below Menthosa peak) to 4353 m above sea level (a.s.l.). Debris covers area covered ∼1.43 km^2 of the ablation surface, with varying thickness from 32 cm to 89 cm (Prakash et al. 2019). It has elevation ranges from 4353 to 6351 m a.s.l., and with mean elevation of 5115 m a.s.l. It has an average slope of 18.8° degree, varying from 72.8° (in the accumulation zone) to a gentle slope (9°) in the ablation area. The mean slope in the lower ablation zone particularly for frontal areas is around 12°. The glacier is a compound type, fed by two tributaries

Table 1. Specification of the satellite datasets used in the study.

Sensor type	Scene ID	Acquisition date	Spatial resolution (m × m)	Image type
Corona KH-4A	DS1024-1023DF102	24/9/1965	4	Pan
Landsat ETM^{+}	LE71470372011271PFS00	28/9/2002	15,30	Multi-spectral
Landsat 8 OLI/TRIS	LC08_L1TP_147037_20131027_20170429_01_T1	27/10/2013	15,30	Multi-spectral
IRS LISS IV	142673731	23/10/2013	5.8	Multi-spectral
Sentinel-2	L1C_T43SFS_A011971_20171007T053044	10/10/2016	10,20	Multi-spectral
ALOS PALSAR	AP_07799_FBD_F0640_RT1	22/08/2015	12.5	DEM
SRTM 1 Arc second	n32_e076_1arc_v3	February, 2000	30	DEM

(Figure 1(b)). The left side tributary is steeper with an average slope of 23.6° as compared to the right side tributary (18.9°). The length of left side tributary from snout is ∼6.7 km which is comparatively higher than from right side tributary (∼5.6 km).

This glacier gives origin to the Urgos Nala (rivulet), approximately 6.4 km in length before its confluences with the Miyar River at Tingrat village. The Miyar River, a major tributary of the Chandra-Bhaga basin (Upper Chenab) in the Lahaul Himalaya, and it joins the Chenab River at Udaipur (∼2600 m a.s.l). In terms of climate, the study area is situated between the monsoon-dominated Pir Panjal to the south and mid-latitude Westerlies-dominated Ladakh to the north of the Great Himalayan Range (Deswal et al. 2017). Therefore, due to the higher topographic characteristic, maximum precipitation normally falls in winter months as snowfall in the region. The annual snowfall and rainfall during 1975–2015 at Indian Meteorological Department (IMD) Udaipur station (about 25 km downstream from the Menthosa Glacier) was observed ∼380.2 cm and ∼323.5 mm, respectively. The climate of the region is semi-arid, therefore melt-water from the seasonal snow and Menthosa Glacier is the only source of water for Urgos village and other nearby downstream villages for agriculture fields, pasture land, domestic use and directly affect the people's livelihood.

3. Database and methods

3.1. Datasets

In the present study, multi-temporal remote sensing datasets were used for the estimation of glacier changes during the past half a century i.e. 1965–2016. Corona KH-4A, Land Remote-Sensing Satellite System, (Landsat) Enhanced Thematic Mapper+ (ETM+)/ Operational Land Imager (OLI), Sentinel 2 A- Multispectral Instrument (MSI), Indian Remote Sensing (IRS) satellite-Linear Imaging Self Scanning-IV (IRS-LISS-IV) images were used to extract glacier boundary and to assess snout and frontal changes since 1965 to 2016. Additionally, the high resolution images available on the Google Earth platform further used to improve the glacier boundary. Most of the images except IRS-LISS IV were obtained from the United States Geological Survey (USGS) Earth Explorer (https://earthexplorer.usgs.gov/) and selected for the end of the ablation period with minimum snow cover and cloud cover, and with a high solar position to avoid shadows (Table 1, Paul and Svoboda 2009). The high-resolution IRS-LISS-IV satellite imagery was procured from the National Remote Sensing Centre, Hyderabad, India. The high to medium-resolution terrain corrected Digital Elevation Model (DEM) data of Advanced Land Observing Satellite and the Phased Array-type L-band Synthetic Aperture Radar (ALOS PALSAR) (https://www.asf.alaska.edu) with 12.5 m spatial resolution and Shuttle Radar

Topography Mission (SRTM Arc-V3) dataset were used to analysis the topographic characteristics and for 3-D visualization purpose. The orthorectified pan-sharpened Landsat-8 OLI imagery (2013) was used as a base image for the co-registration (Landsat TM/ETM+/OLI, Sentinel-2A MSI and LISS-IV) using the projective transformation algorithm inbuilt in the ERDAS IMAGINE 10 by incorporating SRTM V3 DEM. Moreover, the same orthorectified pan-sharpened Landsat-8 OLI imagery (2013) used for image to image rectification of Corona image using the spline georeferencing method inbuilt in the ESRI ArcGIS 10.4. For images co-registration stable river intersections, sharp edges of rocky ridges and visible linear geological structure were used as ground control points.

Recently, the datasets related to ice thickness distribution of all glaciers on Earth are available at ETH data repository and provided as an output of Farinotti et al. (2019) (https://www.research-collection.ethz.ch/handle/20.500.11850/315707). The repository contains a series of compressed folders (.zip-files) providing the ice thickness distribution of individual glaciers including the Himalayan glaciers. They used an ensemble of up to five models (used principles of ice flow dynamics to invert for ice thickness from surface characteristics) to provide a consensus estimate for the ice thickness distribution of ~215,000 glaciers outside the Greenland and Antarctic ice sheets (Huss and Farinotti 2012; Frey et al. 2014; Fürst et al. 2017; Ramsankaran et al. 2018; Farinotti et al. 2019; Maussion et al. 2019). For estimation of thickness distribution of all glaciers, Farinotti et al. (2019) used methods based on mass-conservation approach, ice flow dynamics, basal shear stress, and glacier elevation range from surface topography. We used the composite thickness data of Farinotti et al. (2019) for the Menthosa Glacier, which is estimated by the ensemble of considered five models, to compare and further validate it with in-suite GPR based ice thickness to comprehend the reliability of these modelled estimates for further studies.

3.2. Glacier mapping and associated uncertainty

The Menthosa Glacier has varying surface characteristics from clean ice in the accumulation zone to extensive debris cover areas in the lower ablation zone (Figure 1). Thus the clean ice area was mapped using a well-established semi-automated band ratio method (near-infrared (NIR)/shortwave infrared (SWIR)) whereas debris-covered glacier areas were manually digitized (Paul and Svoboda 2009; Chand and Sharma 2015b). Spectral colour variations and texture differences, presence of ice walls and exposed ice faces, emerging melt-water streams at the terminus were used to identify and map the boundaries and terminus positions of the debris-covered areas of the glacier (Bhambri et al. 2011; Chand and Sharma 2015b). The 2016 outlines served as a basis for the manual adjustment for the other periods. Based on the outlines of the different years, the areal change for the Menthosa Glacier was calculated. Moreover, the frontal change in glacier length was calculated by drawing parallel stripes at a 50 m distance interval along the central flowline (Schmidt and Nüsser 2009; Chand and Sharma 2015a). Due to the irregular shaped glacier front, the recession rate varies, therefore the glacier length change is calculated as the average length from the intersection of the stripes with the glacier outlines and referred to as average length change (Chand and Sharma 2015a). It is well recorded and understood that the glacier boundary drawn from such multi-spatial resolution data sets is subject to several degrees of uncertainty. Therefore, it needs appropriate consideration to determine the accuracy and acceptable value of the results (Paul et al. 2013). The glacier mapping uncertainty from satellite data is calculated based on a buffer around the glacier margins, as suggested by Granshaw and Fountain (2006). As previously suggested, only one side is considered as affected by the shift; therefore, the buffer size was used as half

of the calculated shift produced by mis-registration (Bolch et al. 2010). Buffers were created of 3 m for the IRS LISS-IV, 5 m for Sentinel-2 and 7.5 m for the Landsat ETM + and OLI images by considering the spatial resolution as well as margin of registration error for each. Average mapping uncertainty for the Menthosa Glacier is 1.6% for the 2013 IRS LISS-IV image, 2.9%, 1.5% and 0.9% for the 2002 ETM+, Sentinel-2 (2016) and Corona 1965, respectively. Further, the uncertainty of the length change was calculated using Equation (1) as recommended by Hall et al. (2003).

$$U_e = \sqrt{(p_1)^2 + (p_2)^2} + \text{Ereg} \tag{1}$$

where U_e represents uncertainty and p_1 and p_2 represent images-1 and image-2 pixel resolutions, respectively, the registration error is E_{reg}. Finally, the glacier area change mapping uncertainty was calculated following the multiplication of the uncertainty of glacier length with width, as proposed by Bhambri et al. (2012).

3.3. Climate data and analysis

The IMD snowfall and rainfall data of Udaipur station (~2652 m asl; 32°43′34.31″N–76°39′47.05″E) for the period 1975 to 2015 (40 years) were obtained from district headquarter of Lahaul and Spiti. For long-term climatic trends, we used Climatic Research Unit (CRU) gridded datasets (nearest grid 32.75 N, 76.75 E) for temperature (°C) and precipitation (mm) during the period of 1901 to 2016. It is downloaded from publicly accessible webpage of CRU http://www.cru.uea.ac.uk/. In this gridded dataset station anomalies were interpolated into 0.5° latitude by 0.5° longitude grid cells covering the global terrestrial surface (excluding Antarctica), and combined with an existing climatology to achieve absolute monthly values (Harris et al. 2014). Although gridded data cannot replace in-situ ground and upper air measurements (Chand et al. 2020), due to a lack of ground data, we used it to understand general climatic trends and to compare previously documented climatic trends regionally and at basin scale. Furthermore, similar datasets have been widely used in recent Himalayan glacier studies to understand glacier-climate interactions and to reconstruct the long-term glacier mass balance (Azam et al. 2014; Chand et al. 2017; Mal et al. 2019; Chand et al. 2020). The IMD and CRU gridded data assist to comprehend the response of glacier change to climatic factors.. A commonly used non-parametric Mann–Kendall, Sen's slope estimator and simple linear regression analysis were used to evaluate any statistical trends in climatic data (Mann 1945; Kendall 1975).

3.4. Ice thickness measurement

For in-situ measurement of ice thickness, GPR system normally uses electromagnetic waves in MHz frequency to record the sub-surface areas without boring or trenching (Bohleber et al. 2017). In the present study, we used portable IDS-TR 25 MHz unshielded GPR system. The low-frequency antennas (25–200 MHz) were used for getting deeper profile of ice (Pomerleau et al. 2020). The GPR system we used for the present study is comprised of unshielded antennas, transmitter (Tx) and receiver (Rx), one fast-wave control unit (DAD), battery, network cable and a Toshiba Toughbook (Laptop) for data visualization, storage and processing. The electromagnetic properties of the surveyed materials and antenna frequency determine the penetration depth and resolution of GPR (Jol 2009). On the basis of antennas, resolution normally increases with increasing operating

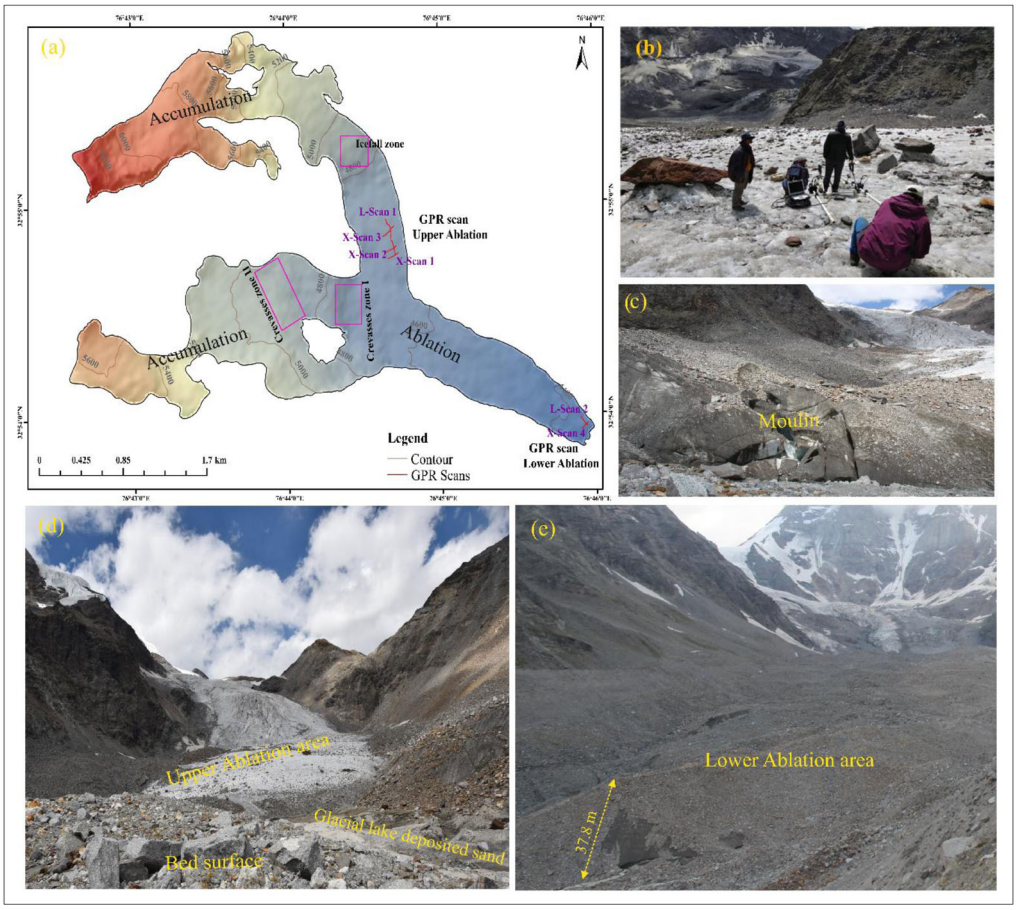

Figure 2. GPR scans on the Menthosa Glacier; (a) GPR scan transect in upper left-side glacier tributary ablation area and lower ablation area with 25–600 MHz dual-frequency antenna; (b) Field photographs of GPR scan transect on the Menthosa Glacier; (c) Recently formed Moulin in upper ablation area; (d and e) Field photographs of GPR scans sections in upper left-side glacier tributary and lower ablation area. The dotted yellow line indicates the height of the Menthosa Glacier frontal part from the base.

frequency and vice versa (McCarthy et al. 2017). While scanning, we considered earlier flagged issues which lead to complications in the GPR studies of the Himalayan glaciers. The GPR surveys were carried out in the upper left side tributary and lower ablation area near the terminus of the Menthosa Glacier (Figure 2). Moreover, the debris thickness measured at different points along with the surveyed GPR profiles and found higher debris cover of 32 to 89 cm in the lower ablation areas near to snout. However, the debris thickness in upper ablation area of left side tributary of the Menthosa Glacier is less than 5–10 cm. This depth information was used for correcting the field measured ice thickness. In the field, before starting the survey, the GPR unit was calibrated by moving from initial line of survey on the glacier surface, where instrument automatically calculated the calibrated distance. Data were acquired using K2 Fast Wave Software (02.00), and GPR data stored in DZT (.dzt) format. All survey parameters were taken into consideration, by following the recommendations specified in the K2 Fast Wave v. 02.00 user manual. In this GPR system, the wheel attachment facility is available, therefore, data collected in continuous profiles (Singh et al. 2010). To make the traverse easier on rough sliding surface,

Table 2. Temporal terminus and frontal area changes of the Menthosa Glacier.

Observation years	Area (error) 10^3 m^2	Annual (error) 10^3 m^2 a^{-1}	Mean terminus (error) M	Annual (error) m a^{-1}
1965–2002	70.4 (±2.7)	1.9 (±0.07)	189.1 (±28.7)	5.1 (±0.78)
2002–2013	17.97 (±3.2)	1.6 (±0.29)	79.9 (± 27.1)	7.3 (±2.5)
2013–2016	4.21 (±2.9)	1.4 (±0.97)	32.5 (± 28.1)	10.8 (±9.4)
1965–2016	92.59 (±2.1)	1.8 (±0.04)	301.5 (± 19.2)	5.9 (±0.4)

a pair of ski sledge was attached underneath of the GPR unit for seamless survey, and also in reducing otherwise obtained errors. In order to reduce the noise, and avoid the problem of fast-slip of this GPR instrument on the glacier ice, the surface scans were obtained at carefully measured speed.

The GPR signal explanation is one of the most challenging tasks because it needs information of the dielectric constant and physical properties of the material (Singh et al. 2017). Therefore, in this study a 3.1 dielectric constant was used for glacier thickness measurement as suggested earlier for the Himalayan glaciers by Singh et al. (2010). Finally, the GPR data were processed using the GRED-HD software of the Ingegneria Dei Sistemi (IDS). In the post-processing operation, different filters were applied to eliminate the noise and improve the radar profiles information to calculate the ice thickness. In particular, a gain correction, DC shift, bandpass and background removal filters were applied to improve weak radar signals (Singh et al. 2018; Kumar et al. 2020). The background removal filter helped to remove transmitter blanking at the top of the reflection profiles due to low-frequency direct wave and bandpass filter effectively removed high-frequency noise (McCarthy et al. 2017). In this study, modelled based estimated ice thickness of Huss and Farinotti (2012), Frey et al. (2014), Fürst et al. (2017), Maussion et al. (2019) and Ramsankaran et al. (2018) was analyzed and composite ice thickness data of Farinotti et al. (2019) of the Menthosa Glacier compared with the field data of GPR profiles. Moreover, the snout area section (i.e. lower ablation area) covered by GPR profiles is not available or mapped in Farinotti et al. (2019) modelled ice thickness dataset of Menthosa Glacier because they used Randolph Glacier Inventory (RGI) glacier outline dataset as an input data for calculation of ice thickness. Therefore, due to inconsistency of RGI Menthosa Glacier outline, current research was unable to compare lower ablation area GPR based ice thickness with modelled ice thickness of Farinotti et al. (2019). In RGI dataset the Menthosa Glacier is mapped as a two glacier (RGI id RGI60-14.18483; RGI60-14.17666), with total area of 4.9 km^2 (RGI Consortium 2017), which is 1.1 km^2 less than actual area of the glacier.

4. Results

4.1. Glacier length change

In the study, last half a century (51 years) snout changes were estimated based on changes observed on the satellite images, along with field measurements since 2006 onwards to present (2017). The repeated photographs for different year since 2006 onwards further support and validate our results derived from multi-temporal satellite images. Our measurements of the average recessional rate and total area vacated for the Menthosa Glacier over time periods from 1965 to 2016 are given in Table 2. We measured an average retreat of 301.5 ± 19.2 m for the Menthosa Glacier from 1965 and 2016, having a varying rate of recession for the different observed periods. For instance, the Menthosa Glacier terminus retreated 189.1 ± 28.7 m (5.1 ± 0.78 m a^{-1}) from 1965 to 2002, 79.9 ± 27.1 m

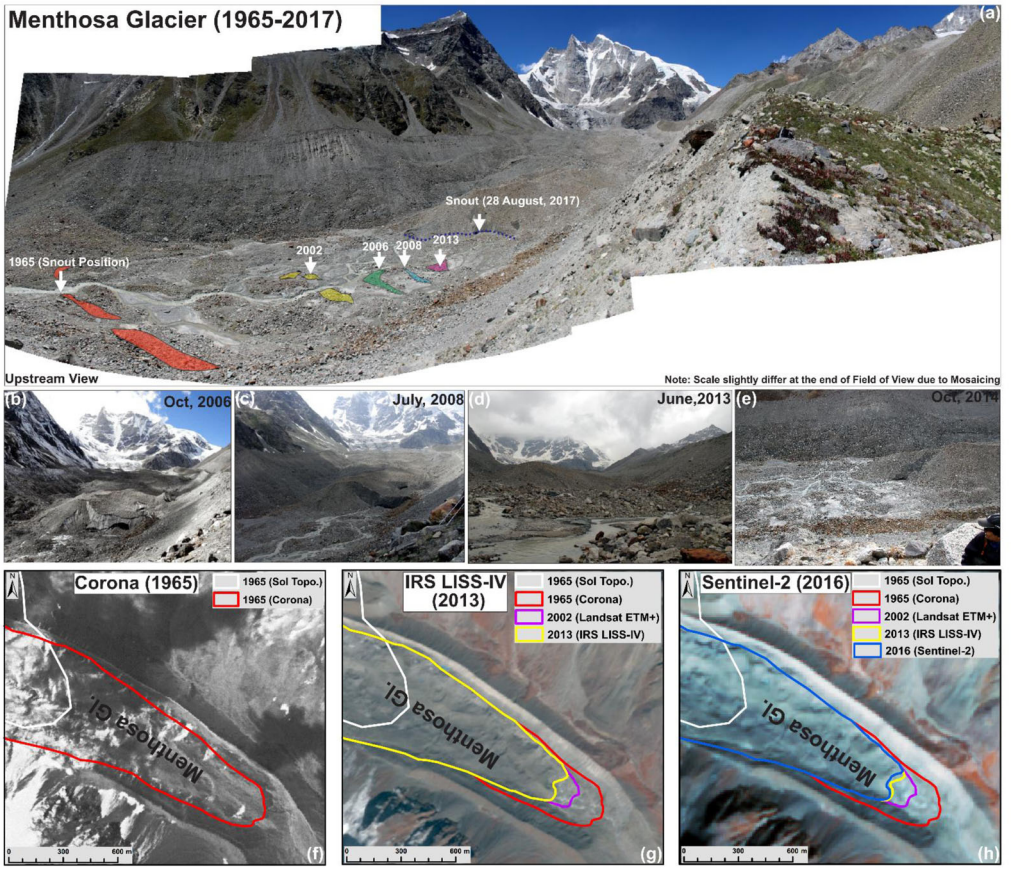

Figure 3. Reconstructed frontal retreat of the Menthosa Glacier (1965–2017); (a) Different colour on the photograph represent the snout position; (b–e) Images shows the snout position of the Menthosa Glacier; (f-h) Frontal retreat of Menthosa Glacier on different satellite images.

(7.3 ± 2.5 m a^{-1}) from 2002 to 2013 and 32.5 ± 28.1 (10.8 ± 9.4 m a^{-1}) m from 2013 to 2016 (Table 2). Moreover, we identified the past terminus and frontal position (1965 and 2000) of the glacier boundary based upon deglaciated features e.g. recessional moraines and relict melt streams in the field with supplement of high to medium resolution satellite images of Corona (1965) and Landsat ETM+ (2000). Accordingly, the identified information transferred into mosaic photograph (2017) for representing the long term recessional history of the Menthosa Glacier pictorially (Figure 3). The glacier terminus position for the years 2006, 2008, 2013 and 2017 was validated in the field, using a handheld Global Positioning System (GPS) and same also transferred into mosaic photograph (2017). The field investigation since 2006 onwards supports the glacier recession trend from remote sensing data.

4.2. Glacier area change

The frontal area changes of the glacier, also show the decreasing trends since the past five decades i.e. 1965–2016 with having a varying rate of change during different observed periods. The total frontal area lost by the glacier for the period between 1965 and 2016 is 0.09 ± 0.002 km^2, about 1.5% of the total loss of the glacier area. Moreover, the glacier lost

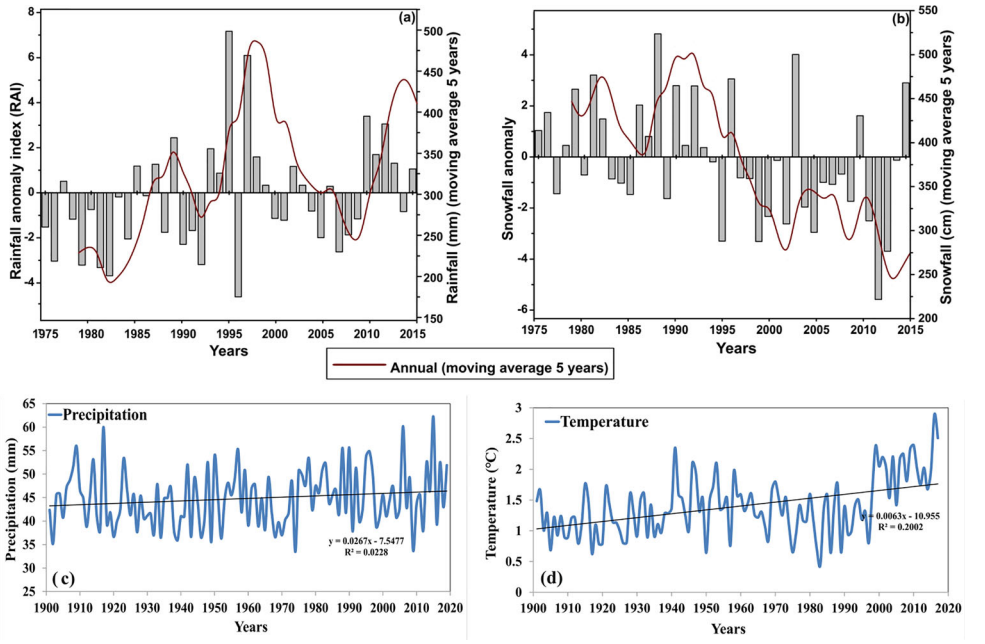

Figure 4. The trend of IMD rainfall and snowfall data of Udaipur during 1975-2015 (a,b); Average annual temperature and precipitation trends for the nearest grid to the Menthosa Glacier (32.75 N, 76.75 E) of CRU (c,d). Note: - CRU gridded datasets are strictly used to capture the general climatic trends in the region.

$0.07 \pm 0.003\,km^2$ of area from 1965 to 2002, $0.02 \pm 0.003\,km^2$ from 2002 to 2013, and $0.004 \pm 0.003\,km^2$ from 2013 to 2016 with having annual area loss of 0.002 ± 0.007, 0.002 ± 0.003 and $0.001 \pm 0.009\,km^2$, respectively (Table 2). As the glacier area has been decreasing, new developments of glacial and deglaciated features observed during the field works, such as exposed rocks, increase in debris cover, newly formed moulin (Figure 2(c)), supraglacial lakes, ice cliffs (Figure 6(e,f)), and ice-marginal lakes were found in areas adjacent to the glacier boundary. The glacier area change of Menthosa Glacier is also associated with relief. Curvatures and slope in Menthosa basin control the movement of the ice/snow flow into different direction, and convex curvature and steep slopes in the upper ablation and accumulation area of the glacier cause diversion of snow masses into small patches and those patches are vulnerable to fast melting. Therefore the higher region of the glacier shows less snow and ice accumulation.

4.3. Climatic trends

The trends in temperature, precipitation and snowfall data of IMD and CRU were analyzed to observe pattern of climate over a period of time in the present study. Nevertheless, the absence of a meteorological station near the glacier makes it challenging to analyze specific glacial basin climatic variability and establish a relationship with glacial change. Therefore, present climatic datasets are strictly used to capture the general climate trends in the region and to elucidate the response of climatic factors on the Menthosa Glacier change. The maximum annual snowfall at Udaipur was recorded at 724.6 cm in 1988. Minimum annual snowfall at Udaipur was recorded at 36.1 cm in 2012. In 1995 highest annual rainfall at Udaipur was recorded 816.54 mm. Study area received maximum rainfall in the monsoon season, and in other months, precipitation occurs in a

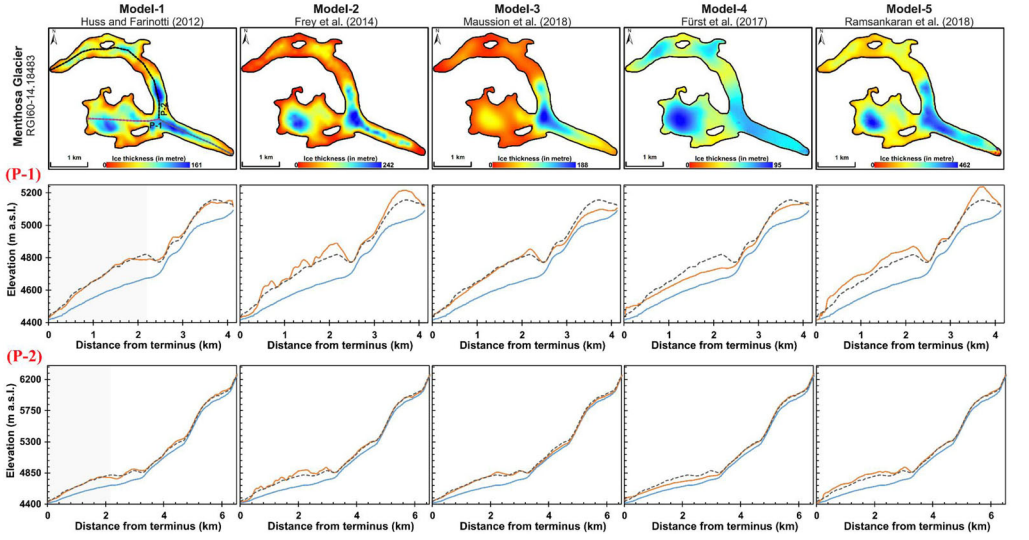

Figure 5. Ice Thickness map of Menthosa Glacier. Profile (P-1) 1 and 2 (P-2) show glacier profile elevation, distance from the snout, and glacier thickness. Below each model P-1, P-2 and bed surface of the Menthosa Glacier (in same model map) with composite model ice thickness are plotted. Blue lines represent bed surface; dotted black line shows composite model thickness and orange line shows each model ice thickness.

solid form. The annual snowfall data of Udaipur show a significant decreasing trend (5.3 $cmyr^{-1}$) during the last four decades (1975–2015) (Figure 4(b)). Similar decreasing trends in snowfall were observed for December, January, February and March (DJFM). However, the rainfall data shows an increasing trend (0.5 $mmyr^{-1}$) in rainfall occurrence during the same period of 1975–2015. It can be mainly ascribed to warming trend as same observed from gridded data in region which principally led to decline in snowfall contribution to total precipitation and it convert to rainfall (Bhutiyani 2016). Overall, reanalyzed datasets of CRU (1901–2016) based on Mann-Kendall and Sen's slope shows an increasing average annual temperature trend (0.006 $°Cyr^{-1}$), whereas annual precipitation shows an insignificant trend (Figure 4(c,d)). The rate of increased trend in temperature is significant because a slight change in temperature has impact on the fluctuation of glacier and needs further investigation.

4.4. GPR measured ice thickness and modelled ice thickness

GPR surveys were conducted during 2016 (lower ablation area) and 2017 (upper left tributary part of ablation area). Six GPR profiles were taken and surveyed over the Menthosa Glacier, four profiles in the upper left tributary part, and two in the lower ablation area of the glacier. Out of six, two profiles are longitudinal; one in upper ablation and one in lower ablation area and four transverse profiles; three in the upper and one in the lower ablation area (Figure 2). In general, glacier thickness is influenced by mean slope, and it is expected that steeper the glacier, thinner the ice and vice versa (Singh et al. 2018). Glacier bed surface profiles obtained from remote sensing methods, GPR and other field methods can be used for the reconstruction of glacier thickness and topographic information of the glacier bed. GPR profiles quantified that the glacier-ice thickness ranges from 24 meters at the lower part, and gradually increases to about 55 meters at the thickest protruding part in the upper ablation area of the Menthosa Glacier. The GPR based estimated ice thickness in the lower ablation area varies from 38 to 42 meters.

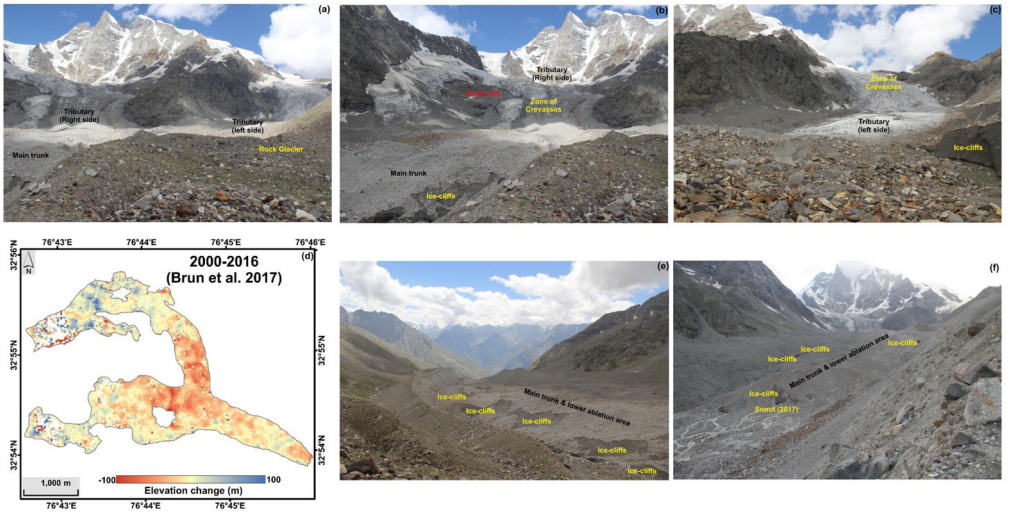

Figure 6. Field photograph of glacier surface and topographical characteristics; (a–c) Ice thickness along the steep and gentle slope and crevasses zone; (e,f) Formation of series of ice-cliff in the ablation zone; (d) The significant change in glacier's surface elevation and overall mass balance of the Menthosa Glacier during 2000-2016 (Brun et al. 2017).

The lower ablation area is covered with thick debris, making it challenging to take GPR profile for a large area. Hence two GPR profiles were taken and surveyed in this area. Radargrams in the lower ablation area contain more hyperbolic signatures and noises that may be due to boulders and high debris thickness. In spite of all the limitations, ice thickness of the glacier was assessed successfully by using filtering options in inbuilt processing software.

In the Farinotti et al. (2019) all five models used DEM based glacier's surface topography, and principles of ice flow dynamics. Thereafter, composite thickness was calculated against observations in a cross-validation scheme, and inverse variance and bias weighting. The composite thickness method provides mean ice thickness because it is relies on all other five models. Highest ice thickness of Menthosa Glacier found in the composite thickness estimation model was 150 meters, whereas the other five models show highest ice thickness between 95 and 462 meters. Interestingly, it observed that the ablation area of the Menthosa Glacier is thicker than the accumulation area, as the ablation zone lies in a trough, and accumulation area is on steep slopes of the mountain. To understand the ice thickness of the glacier and its tributaries, we drawn two profiles for ice thickness measurement of the glacier (Figure 5). In all five models ice thickness pattern looks similar, but quantitatively there are large variations among all and also show deviation from composite thickness model (Figure 5). Different coloured line profiles were drawn to show the deviation (Figure 5, P-1 & P-2). Profile-1 (P-1) represents the right side and Profile-2 (P-2) represents the left side of the glacier tributaries. Approximately all models show deviations from the mean (composite) ice thickness and can be observed visually in Figure 5. However, models 1 and 3 show less ice thickness deviation with composite model as compared to other Models. In all models, P-1 shows that there is a slight increase in ice thickness from altitude of ~4700 m (after crevasses zone-I). After crevasses zone-II there is a sharp increase in ice thickness and it decreases towards the peak of Menthosa. P-2 indicates that below and after the icefall of the glacier, there is a slight increase in ice thickness (Figure 5). It is evident from these profiles that the central zone

of the glacier is thickest, as compared to the upper and lower parts of the glacier. This difference is due to the fact that the upper parts of Menthosa lie on steep slopes and the lower parts are having gentle slope and experienced melting. The ice thickness found in composite model near the terminus is ~17-25 meters, in the middle part of the glacier it is between ~100 to ~150 meters, and in the upper area it is ~30 to ~65 meters.

Field photographs taken for different parts of the glacier also show that the upper region has a steep slope (Figure 6), and the same can be visualized in topography profiles shown in Figure 1. Likewise, over the middle region of the glacier (i.e. between 4650 m a.s.l. and 4750 m a.s.l.) which is characterized by moderate to lesser slope, relatively higher ice thickness is observed (Figure 6).

5. Discussion

5.1. Frontal retreat and comparison with other glaciers in the region

Menthosa Glacier has receded by 301.5 ± 19.2 m, from 1965 to 2016 (51 years), with an average annual retreat of 5.9 ± 0.4 m a^{-1}. During this period, the total ice lost by the glacier is 0.09 ± 0.002 km^2 (0.002 ± 0.004 km^2 a^{-1}), which is 1.5% of the total glacier area. The multi-temporal satellite images from 1965 onwards, recent repeated photographs of 2006 to 2017 and field observations also suggest that the glacier has receded over the period of time. The ablation zone of Menthosa Glacier is covered under thick debris cover and annual rate of retreat was estimated 5.9 ± 0.4 m (1965–2016), which is similar to the reported rate of retreat (7.3 ± 0.7 ma^{-1}) of extensive debris covered Batal Glacier by Sharma et al. (2016). Although, the mean terminus and annual rate of retreat of Menthosa Glacier varied significantly across observational time periods (Table 2). In addition to this Birajdar et al. (2014), Deswal et al. (2017), Pandey and Venkataraman (2013), Chand et al. (2017) and Patel et al. (2018) also reported glacier retreat in the region. Pandey and Venkataraman (2013) reported that in 30 years (1980 to 2010), glaciers terminuses in the Chandra–Bhaga basin retreated at an average of 465.5 ± 169.1 m with an annual retreat rate of 15.5 ± 5.6 m. For the same time period (1965 and 2014) Chand et al. (2017) estimated the average total retreat of the Bara Shigri Glacier was 1100.2 + 32.1 m with an annual rate of 22.5 + 0.7 m. In the Miyar basin Patel et al. (2018) reported an average terminus retreat of 29 glaciers was 243 ± 125 m with annual retreat rate of 9.6 ± 5.2 m from 1989 to 2014. Overall our results of the Menthosa Glacier recession and frontal area change are in good agreement with reported recession rate for other glaciers nearby and adjoining basins (Chand et. al. 2019)

5.2. Influence of climatic factors

The annual average temperature for the nearest grid point of CRU data shows significant warming trends, with some cyclic drifts. The Udaipur IMD data shows a significant (confidence level > 95%) decreasing trend in annual snowfall and an increasing trend in rainfall during the 1975 to 2015. In the region, previous studies reported increasing trends for temperature and decreasing trends for precipitation for the same time period (Chand et al. 2017; Kaushik et al. 2020). Chand et al. (2017) based on IMD data (1975–2010) and reanalysis data (1948–2014), reported decreasing trends for precipitation, annual snowfall and rainfall, and increasing trends for temperature. In the Bhaga basin Kaushik et al. (2020) reported an increasing rate of 0.021 °C yr^{-1} for temperature (1961–2015) and decreasing rete of −2.724 $mmyr^{-1}$ for precipitation (1951–2015). Azam et al. (2012) and

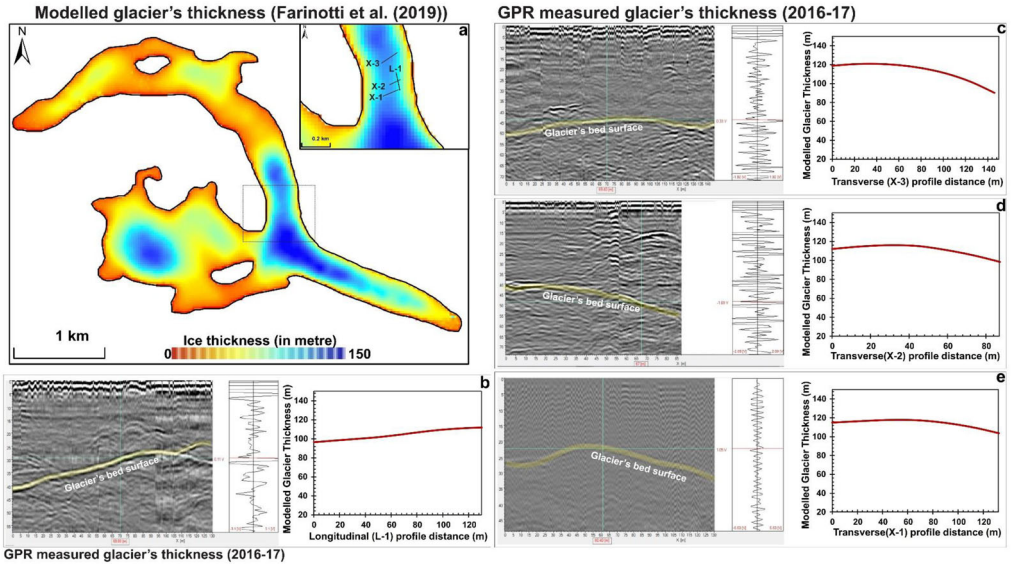

Figure 7. (a) Composite ice thickness map of Menthosa, after Farinotti et al. (2019), inset to the top right is the location of GPR survey section in upper ablation area; (b–e) Composite model ice thickness compared with GPR measured ice thickness; Radargrams of upper ablation area and red line profiles represent ice thickness of same sections on the composite ice thickness map.

Vincent et al. (2013) also reported that negative mass balance of the Chhota Shigri glacier is due to rise in temperature and decrease in snowfall. Considering these climatic trends in the study area, the retreating behaviour of glaciers in the region is noticeably reveals climate dependency.

5.3. Comparison of the modelled ice thickness assessments with GPR field assessments

In this study, modelled based ice thickness was verified with the in-situ measurements carried out through GPR profiling. GPR results compared with composite ice thickness model dataset because in the model random errors are minimized in ensemble approach, all aspects taken into consideration through spatial smoothing of individual model outputs and well captured mean thickness in this dataset. In the upper left side tributary ablation area of the glacier, a longitudinal scan (L-1) with total length of 130 m was carried out from the upper to lower part of the glacier because of ease to move GPR instrument downslope on a ski-sledge. This longitudinal radargram shows a continuous decrease in the ice depth from 41 to 28 meters at the termination of GPR scan (Figure 7(b)). For the same section ice thickness measured in the composite model is 88 to 105 meters. The first transverse GPR profile (X-scan 1) in this upper ablation area shown 24 to 30 meters average depth of glacier-ice (Figure 7(e)). For same section ice thickness measured in the composite model is 100 to 106 meters. Moreover, the field evidence and photographs supported the GPR based measurement of 24–30 meters because the presence of ice-marginal lakes adjoining to the glacier boundary and exposure of bed surface in downward side (Figure 2(d)and Figure 6(c)). The second profile (X-scan 2) 87 m long shows an increase in the glacier depth from 40 to 55 meters (Figure 7(d)). For the same section ice thickness measured in the composite model is 96 to 106 meters. The third 144 m long transverse profile closer to the icefall (X-scan 3) shows thicker and continuous

ice depth (47–51 meters) as compared to the X-scan 1 and X-scan 2 GPR profiles (Figure 7(c)). For same segment ice thickness measured in the composite model is 84 to 120 meters. The ice thickness estimated in the model for the icefall section (steep slope section) is approximately 50 metres, but based on field observations and photographs it appears to be approximately double the actual ice thickness (Figure 6(a–c)).

The longitudinal profile (L-scan 2 in Figure 2(a)) 67 m long in the lower ablation area of the glacier was taken from the crest of the snout of the Menthosa Glacier to upward. The longitudinal profile shows continuous increase in glacier depth from ∼38 to ∼45 meters. Cross-verification of the ice thickness at the snout (lower ablation) was carried out using a digital hypsometer and Total Station in 2017 (Prakash et al. 2019), yielded ∼37.8 meters (tilt area also accounted for this value), which also supporting GPR measured ice depth in L-scan 2. The transverse profile (X-scan 4) has captured almost similar depth of ice in the lower ablation area. During the survey, it was also observed that the surface of the glacier in this section was flat throughout the scan. This profile shows a constant depth of 43 m in lower ablation area of Menthosa Glacier (Supplementary figure 1(b)). Correspondingly in the Chandra-Bhaga river basin, Swain et al. (2018) using GPR reported ice thickness in accumulation area (at 4600 m a.s.l) of extensively debris-covered Hamtah Glacier (an area of 3.24 km^2 and 6 km long) was 35 to 95 meters and thickness measured for ablation area (4070–4300 m a.s.l) 20 to 40 meters. Azam et al. (2012) reported ice thickness of less debris-covered Chhota Shigri Glacier (an area of 15.7 km^2 and 9 km long) along centre-line from was 124 meters (at 4400 m a.s.l) to 270 meters (at 4900 m a.s.l.).

5.4. Limitation and recommendation

In the present study, comparison was made between the modelled ice thickness estimates and GPR based ice thickness measurements. However, it is to be noted that the modelled estimates for the glaciers in Indian Himalayas were not validated using corresponding field measurements (Huss and Farinotti 2012; Frey et al. 2014; Farinotti et al. 2017). Generally, the difference in timestamps between these modelled estimates and the field measurements available in the Himalayas are in decadal range and hence cast doubts on the reliability of the modelled estimates. Moreover, the models mentioned in Farinotti et al. (2019) used freely available SRTM 90 m DEM for Himalayan glaciers and a common shape factor parameter. Thus consider into this fact, we avoid to directly compare the modelled ice thickness estimates with GPR based ice thickness measurements. We first calculated the surface elevation change for each surveyed profile of the Menthosa Glacier from available glacier's surface elevation change (2000–2016) datasets of Brun et al. (2017). Accordingly, the problem of readability in terms of difference in timestamps (2000–2016) between these modelled estimates and the field measurements solved before calculating the Root Mean Square Error (RMSE). In the study, RMSE is estimated between 38 to 72 ± 10 m which is almost similar to the previous study by Frey et al. (2014) of 60.7 m for the Huss and Farinotti (HF) and 63.7 m for GlabTop2 model. The higher value of RMSE indicates modelled ice thickness suffer from model parameterisation scheme and availability of accurate and high-resolution DEM. Moreover, the shape factor and surface slope are highly sensitive input data in these models (Haq et al. 2021). In addition, other input data like quality of DEM, void in DEM data, glaciers outline inaccuracy and spatial smoothing of calculated ice thickness affect the accuracy of remote sensing calculated ice thickness (Vijay and Braun 2016; Maurer et al. 2019). Therefore field-based GPR measured ice thickness is effective to measure glacier ice thickness and

bottom topography (Mishra et al. 2018), accurate assessment of water volumes in the glacier (Singh et al. 2019), and for monitoring of future glacier dynamics (Colombero et al. 2019). However, GPR measurements also suffer from some limitations; conducting GPR survey is very difficult in the glaciers of the Himalayan region because of harsh climate, rugged terrain, and crevasses (Singh et al. 2017). In addition, a high amount of noises and sudden changes in the amplitude of the signal were observed because of sudden changes in glacier ice, crevasses, supraglacial melt-water channels and surface debris cover (Liu et al. 2020). These sudden changes in signal and noises affect the accuracy of GPR calculated ice thickness. Therefore to overcome these limitations, single glacier airborne thorough GPR surveys with physical verified observation can be conducted in mountainous environment. Keeping all the above facts in mind, modelled ice thickness derived from remotely sense is more robust and suitable if it should be used glacier specific model parameterization scheme and relatively accurate and high-resolution DEM with GPR validation for different varying characteristics glaciers across the Himalayan region.

6. Conclusions

This study provides a comprehensive analysis of Menthosa Glacier on ice thickness, frontal retreat and area changes during the past half a century (1965–2016) and evaluated its response to the climatic conditions. There is unequivocal evidence for the frontal recession and area change observed since 1965, a trend much similar to the rest of the glaciers in the region. It was observed that Menthosa Glacier has receded by 301.5 ± 19.2 m during the last 51 years (1965–2016), with an average annual retreat rate of 5.9 ± 0.4 m , whereas for the same period area loss of 0.09 km^2 was measured. The multi-temporal satellite analysis are also supported by repeated field photographs and observations since last decades (2006–2017). The climatic parameters trends of snowfall, rainfall and temperature established the relationship of glacier recession in response to climate warming and decreased snowfall. For instance, a decreasing trend of snowfall over the past four decades and increasing trend of temperature over the past century has resulted impact on the retreat of the glacier. The modelled ice thickness obtained for the Menthosa Glacier is measured ~17 to 150 meters, which is overestimated and in some cases almost double to the depth obtained in GPR profiles. It can be ascribed to certain uncertainties, like model parameterization scheme and uncertainty (e.g. used common shape factor parameter), input data uncertainty, and some case difference in timestamps between these modelled estimates and the field measurements therefore it is recommended to validate the same from GPR data of the selected glaciers with varying surface and topographical characteristics. The frontal ice thickness of glacier obtained at snout in the lower abalation zone using GPR scan comes closer to the one measured by the Total Station and digital hypsometer, thus validating the usefulness of each of these techniques for glacier's ice thickness studies. Furthermore, the GPR measured ice thickness for the Menthosa Glacier shall be valuable to fill the substantial gaps in field-based ice thickness knowledge exist for the Himalayan glaciers (GlaThiDa Consortium 2019) and contribute to improve the existing models of ice thickness estimation for varying characteristics of the glaciers across the Himalayan and other part of the world.

Acknowledgments

This work was financially supported by the Department of Science and Technology and the Space Applications Centre/ISRO Ahmadabad, Government of India, over 2013–2019. We are thankful to

anonymous reviewers and the editorial board for providing constructive comments and suggestions which helped us to improve the content of the manuscript. The authors are thankful to the Jawaharlal Nehru University, New Delhi (India) for providing research facility and infrastructure. We also would record our thanks to Mr Satish Kumar, and Tenzin Dorje for assistance in the GPR & GPS surveys. Our special thanks to the villagers of Urgos and Tingrit for extending logistical support all this while. The authors acknowledge the USGS for providing satellite data except IRS LISS-IV for this research at free of cost. Pritam Chand is grateful to the Central University of Punjab, Bathinda (India).

Disclosure statement

No potential conflict of interest was reported by the author(s).

ORCID

Pritam Chand http://orcid.org/0000-0001-7388-0393
Vijendra Kumar Pandey http://orcid.org/0000-0002-2384-317X

References

Azam MF, Wagnon P, Patrick C, Ramanathan A, Linda A, Singh VB, 2014. Reconstruction of the annual mass balance of Chhota Shigri glacier, Western Himalaya, India, since 1969. Ann Glaciol. 55(66): 69–80.

Azam MF, Wagnon P, Ramanathan A, Vincent C, Sharma P, Arnaud Y, Linda A, Pottakkal JG, Chevallier P, Singh VB, et al. 2012. From balance to imbalance: a shift in the dynamic behaviour of Chhota Shigri glacier, western Himalaya. J Glaciol. 58(208):315–324.

Bhambri R, Bolch T, Chaujar RK, 2012. Frontal recession of Gangotri Glacier, Garhwal Himalayas, from 1965–2006, measured through high resolution remote sensing data. Curr Sci. 102(3):489–494.

Bhambri R, Bolch T, Chaujar RK, Kulshreshtha SC, 2011. Glacier changes in the Garhwal Himalaya, India, from 1968 to 2006 based on remote sensing. J Glaciol. 57(203):543–556.

Bhutiyani MR. 2016. Spatial and temporal variability of climate change in high-altitude regions of NW Himalaya, in climate change. In: RB Singh, U Schickhoff, S. Mal, editors. Climate Change, Glacier response, and vegetation dynamics in the Himalaya. Cham (Switzerland): Springer; p. 87–101.

Birajdar F, Venkataraman G, Bahuguna I, Samant H, 2014. A revised glacier inventory of Bhaga Basin Himachal Pradesh, India: current status and recent glacier variations. ISPRS Ann Photogramm Remote Sens Spat Inf Sci. II(8):37–43.

Bohleber P, Sold L, Hardy DR, Schwikowski M, Klenk P, Fischer A, Sirguey P, Cullen NJ, Potocki M, Hoffmann H, et al. 2017. Ground-penetrating radar reveals ice thickness and undisturbed englacial layers at Kilimanjaro's Northern Ice Field. Cryosphere. 11(1):469–482.

Bolch T, Kulkarni A, Kääb A, Huggel C, Paul F, Cogley JG, Frey H, Kargel JS, Fujita K, Scheel M, et al. 2012. The state and fate of Himalayan glaciers. Science 336(6079):310–314.

Bolch T, Menounos B, Wheate R, 2010. Landsat-based inventory of glaciers in western Canada, 1985-2005. Remote Sens Environ. 114(1):127–137.

Brun F, Berthier E, Wagnon P, Kääb A, Treichler D, 2017. A spatially resolved estimate of High Mountain Asia glacier mass balances, 2000-2016. Nat Geosci. 10(9):668–673.

Chand P, Jain SK, Thakur HP, Kumar S, Sharma MC, 2020. Recessional pattern and surface elevation change of the Parvati Glacier, North-Western Himalaya (1965-2018) using remote sensing. Int J Remote Sens. 41(24):9360–9392.

Chand P, Sharma MC. 2015a. Frontal changes in the Manimahesh and Tal Glaciers in the Ravi Basin, Himachal Pradesh, Northwestern Himalaya (India), between 1971 and 2013. J Remote Sens. 36(16): 4095–4113.

Chand P, Sharma MC, 2015b. Glacier changes in the Ravi Basin, North-Western Himalaya (India) during the Last Four Decades (1971–2010/13). Glob Planet Change. 135:133–147.

Chand P, Sharma MC, Baruah UD, Deswal S, Latief SU, Saini R, Kumar P, Prakash S, Kumar P, 2019. Shrinking Glaciers of the Himachal Himalaya: A Critical Review. In: A Saikia, P Thapa, editors. Environmental Change in the Himalayan Region. Cham: Springer.

Chand P, Sharma MC, Bhambri R, Sangewar CV, Juyal N, 2017. Reconstructing the pattern of the Bara Shigri Glacier fluctuation since the end of the Little Ice Age, Chandra valley, north-western Himalaya. Prog Phys Geogr. 41(5):643–675.

Colombero C, Comina C, De Toma E, Franco D, Godio A, 2019. Ice thickness estimation from geophysical investigations on the terminal lobes of Belvedere Glacier (NW Italian Alps). Remote Sens. 11(7): 1–19.

Deswal S, Sharma MC, Saini R, Chand P, Juyal N, Singh I, Srivastava P, Ajai, Bahuguna I, 2017. Late Holocene glacier dynamics in the Miyar Basin, Lahaul Himalaya, India. Geosciences. 7(3):64.

Farinotti D, Brinkerhoff DJ, Clarke GKC, Fürst JJ, Frey H, Gantayat P, Gillet-Chaulet F, Girard C, Huss M, Leclercq PW, et al. 2017. How accurate are estimates of glacier ice thickness? Results from ITMIX, the Ice Thickness Models Intercomparison eXperiment. Cryosphere. 11(2):949–970.

Farinotti D, Huss M, Fürst JJ, Landmann J, Machguth H, Maussion F, Pandit A, 2019. A consensus estimate for the ice thickness distribution of all glaciers on Earth. Nat Geosci. 12(3):168–173.

Frey H, Machguth H, Huss M, Huggel C, Bajracharya S, Bolch T, Kulkarni A, Linsbauer A, Salzmann N, Stoffel M, 2014. Estimating the volume of glaciers in the Himalayan-Karakoram region using different methods. Cryosphere. 8(6):2313–2333.

Fürst JJ, Gillet-Chaulet F, Benham TJ, Dowdeswell JA, Grabiec M, Navarro F, Pettersson R, Moholdt G, Nuth C, Sass B, et al. 2017. Application of a two-step approach for mapping ice thickness to various glacier types on Svalbard. Cryosphere. 11(5):2003–2032.

Gärtner-Roer I, Nussbaumer SU, Hüsler F, Zemp M, 2019. Worldwide assessment of national glacier monitoring and future perspectives. Mt Res Dev. 39(2):A1–A11.

GlaThiDa Consortium. 2019. Glacier Thickness Database 3.0.1. Zurich (Switzerland): World Glacier Monitoring Service.

Granshaw FD, Fountain AG, 2006. Glacier change (1958-1998) in the North Cascades National Park Complex, Washington, USA. J Glaciol. 52(177):251–256.

Hall DK, Bayr KJ, Schöner W, Bindschadler RA, Chien JYL, 2003. Consideration of the errors inherent in mapping historical glacier positions in Austria from the ground and space (1893-2001). Remote Sens Environ. 86(4):566–577.

Haq MA, Azam MF, Vincent C. 2021. Efficiency of artificial neural networks for glacier ice-thickness estimation: a case study in western Himalaya, India. J Glaciol.:1–14. DOI:10.1017/jog.2021.19

Harris I, Jones PD, Osborn TJ, Lister DH, 2014. Updated high-resolution grids of monthly climatic observations – the CRU TS3. 10 Dataset. Int J Climatol. 34(3):623–642.

Huss M, Farinotti D, 2012. Distributed ice thickness and volume of all glaciers around the globe. J Geophys Res Earth Surf. 117(4):1–10.

Immerzeel WW, Beek LPH, Bierkens MFP, 2010. Climate change will affect the Asian water towers. Science. 328(5984):1382–1385.

Jol HM. 2009. Ground penetrating radar: theory and applications. London (UK): Elsevier.

Kaushik S, Dharpure JK, Joshi PK, Ramanathan AL, Singh T, 2020. Climate change drives glacier retreat in Bhaga basin located in Himachal Pradesh, India. Geocarto Int. 35(11):1179–1198.

Kendall MG. 1975. Rank correlation methods. 3rd ed. New York (NY): Hafner Publishing Company; p. 128.

Kumar A, Negi HS, Kumar K, Kanda N, Singh KK, Pandit A, Ramsankaran R, 2020. Estimation of recent changes in thickness and mass balance of the Patsio glacier in the Great Himalayan region using geodetic technique and ancillary data. Geocarto Int. 35(1):47–63. DOI:10.1080/10106049.2018.1506506.

Latief SU, Rashid SM, Singh R, 2016. Impact analysis of climate change on Kolahoi glacier in Liddar Valley, Northwestern Himalayas. Arab J Geosci. 9(18):1–15.

Liu J, Wang S, He Y, Li Y, Wang Y, Wei Y, Che Y, 2020. Estimation of ice thickness and the features of subglacial media detected by ground penetrating radar at the baishui river glacier no. 1 in Mt. Yulong, China. Remote Sens. 12(24):1–23.

Mal S, Mehta M, Singh RB, Schickhoff U, Bisht MPS, 2019. Recession and morphological changes of the debris-covered Milam Glacier in Gori Ganga valley, Central Himalaya, India, derived from satellite data. Front Environ Sci. 7:1–17.

Mann HB, 1945. Non-parametric tests against trend. Econometrica. 13(3):245–259.

Maurer JM, Schaefer JM, Rupper S, Corley A, 2019. Acceleration of ice loss across the Himalayas over the past 40 years. Sci Adv. 5(6):eaav7266.

Maussion F, Butenko A, Champollion N, Dusch M, Eis J, Fourteau K, Gregor P, Jarosch AH, Landmann J, Oesterle F, et al. 2019. The Open Global Glacier Model (OGGM) v1.0. Geosci Model Dev. 12(3): 909–931.

McCarthy M, Pritchard H, Willis I, King E, 2017. Ground-penetrating radar measurements of debris thickness on Lirung Glacier. J Glaciol. 63(239):543–555.
Mehta M, Dobhal DP, Bisht MPS, 2011. Change of Tipra glacier in the Garhwal Himalaya, India, between 1962 and 2008. Prog Phys Geogr. 35 (6):721–738.
Mishra A, Negi BDS, Banerjee A, Nainwal HC, Shankar R, 2018. Estimation of ice thickness of the Satopanth Glacier, Central Himalaya using ground penetrating radar. Curr Sci. 114(04):785–791.
Nuimura T, Sakai A, Taniguchi K, Nagai H, Lamsal D, Tsutaki S, Kozawa A, Hoshina Y, Takenaka S, Omiya S, et al. 2015. The GAMDAM glacier inventory: a quality-controlled inventory of Asian glaciers. Cryosphere. 9(3):849–864.
Pandey P, Venkataraman G, 2013. Changes in the glaciers of Chandra–Bhaga basin, Himachal Himalaya, India, between 1980 and 2010 measured using remote sensing. Int J Remote Sens. 34(15):5584–5597.
Patel LK, Sharma P, Fathima TN, Thamban M, 2018. Geospatial observations of topographical control over the glacier retreat, Miyar basin, Western Himalaya, India. Environ Earth Sci. 77(5):1–12.
Paul F, Barrand NE, Baumann S, Berthier E, Bolch T, Casey K, Frey H, Joshi SP, Konovalov V, Le Bris R, et al. 2013. On the accuracy of glacier outlines derived from remote-sensing data. Ann Glaciol. 54(63): 171–182.
Paul F, Svoboda F, 2009. A new glacier inventory on southern Baffin Island, Canada, from ASTER data: I. Applied methods, challenges and solutions. Ann Glaciol. 50(53):11–21.
Pomerleau P, Royer A, Langlois A, Cliche P, Courtemanche B, Madore JB, Picard G, Lefebvre É, 2020. Low cost and compact FMCW 24 GHz radar applications for snowpack and ice thickness measurements. Sensors. 20(14):3909–3929.
Prakash S, Sharma MC, Shahnawaz Pandey VK, Chand P, Deswal S, 2019. Mapping glacial geomorphology and livelihood resources in Urgos Watershed, Lahul and Spiti District, Himachal Pradesh, India. J Indian Soc Remote Sens. 47:1295–1305.
Pratap B, Dobhal DP, Bhambri R, Mehta M, Tewari VC, 2016. Four decades of glacier mass balance observations in the Indian Himalaya. Reg Environ Change. 16(3):643–658.
Qiao B, Yi C, 2017. Reconstruction of Little Ice Age glacier area and equilibrium line attitudes in the central and western Himalaya. Quat Int. 444:65–75. http://dx.doi.org/10.1016/j.quaint.2016.11.049.
Ramsankaran R, Pandit A, Azam M, 2018. Spatially distributed ice-thickness modelling for Chhota Shigri Glacier in western Himalayas, India. Int J Remote Sens. 39(10):3320–3343.
RGI Consortium. 2017. Randolph Glacier Inventory – a dataset of global glacier outlines: 655 version 6.0: technical report. Global land ice measurements from space, Boulder, 656 Colorado, USA. Digital Media. 657 [accessed 2020 September 25]. http://www.glims.org/RGI/randolph60.html.
Scherler D, Bookhagen B, Strecker MR, 2011. Spatially variable response of Himalayan glaciers to climate change affected by debris cover. Nature Geosci. 4(3):156–159. http://dx.doi.org/10.1038/ngeo1068.
Schmidt S, Nüsser M, 2009. Fluctuations of Raikot glacier during the past 70 years: a case study from the Nanga Parbat Massif, Northern Pakistan. J Glaciol. 55 (194):949–959.
Sharma P, Patel LK, Ravindra R, Singh A, Mahalinganathan K, Thamban M, 2016. Role of debris cover to control specific ablation of adjoining Batal and Sutri Dhaka glaciers in Chandra Basin (Himachal Pradesh) during peak ablation season. J Earth Syst Sci. 125(3):459–473.
Shekhar M, Bhardwaj A, Singh S, Ranhotra PS, Bhattacharyya A, Pal AK, Roy I, Martín-Torres FJ, Zorzano MP, 2017. Himalayan glaciers experienced significant mass loss during later phases of little ice age. Sci Rep. 7(1):1–14.
Singh D, Sen Tangri AK, Kumar D, Dubey CA, Bali R, 2017. Pattern of retreat and related morphological zones of Gangotri Glacier, Garhwal Himalaya, India. Quat Int. 444:172–181. http://dx.doi.org/10.1016/j.quaint.2016.07.025.
Singh KK, Kulkarni AV, Mishra VD, 2010. Estimation of glacier depth and moraine cover study using ground penetrating radar (GPR) in the Himalayan region. J Indian Soc Remote Sens. 38(1):1–9.
Singh KK, Negi HS, Kumar A, Kulkarni AV, Dewali SK, Datt P, Ganju A, Kumar S, 2017. Estimation of snow accumulation on Samudra Tapu glacier, Western Himalaya using airborne ground penetrating radar. Curr Sci. 112(06):1208–1218.
Singh KK, Negi HS, Singh DK, 2019. Assessment of glacier stored water in Karakoram Himalaya using satellite remote sensing and field investigation. J Mt Sci. 16(4):836–849.
Singh KK, Singh DK, Negi HS, Kulkarni AV, Gusain HS, Ganju A, Babu Govindha Raj K, 2018. Temporal change and flow velocity estimation of Patseo glacier, Western Himalaya, India. Curr Sci. 114(04):776–784.
Swain AK, Mukhtar MA, Majeed Z, Shukla SP, 2018. Depth profiling and recessional history of the Hamtah and Parang glaciers in Lahaul and Spiti, Himachal Pradesh. Geol Soc Lond Spec Publ. 462(1): 35–49.

Tawde SA, Kulkarni AV, Bala G, 2019. An assessment of climate change impacts on glacier mass balance and geometry in the Chandra Basin, Western Himalaya for the 21st century. Environ Res Commun. 1(4):041003.

Vijay S, Braun M, 2016. Elevation change rates of glaciers in the Lahaul-Spiti (Western Himalaya, India) during 2000-2012 and 2012-2013. Remote Sens. 8(12):1–16.

Vincent C, Ramanathan A, Wagnon P, Dobhal DP, Linda A, Berthier E, Sharma P, Arnaud Y, Azam MF, Jose PG, et al. 2013. Balanced conditions or slight mass gain of glaciers in the Lahaul and Spiti region (northern India, Himalaya) during the nineties preceded recent mass loss. Cryosphere. 7(2):569–582.

Xu J, Grumbine RE, Shrestha A, Eriksson M, Yang X, Wang YUN, Wilkes A, 2009. The melting Himalayas: cascading effects of climate change on water, biodiversity, and livelihoods. Conserv Biol. 23(3):520–530.

Yao T, Thompson L, Yang W, Yu W, Gao Y, Guo X, Yang X, Duan K, Zhao H, Xu B, et al. 2012. Different glacier status with atmospheric circulations in Tibetan Plateau and surroundings. Nat Clim Change. 2(9):663–667.